lubricants

Article

Synergistic Lubrication Mechanism of Nano-Fluid and Grinding Wheel Prepared by CNTs@T304 Nano-Capsules

Jiju Guan [1,*], Zhengbing Zhu [1], Lanyu Yang [1], Yu Xia [2], Xuefeng Xu [2] and Shuiquan Huang [3,*]

[1] College of Mechanical Engineering, Changshu Institute of Technology, Suzhou 215500, China; zhuzb@cslg.edu.cn (Z.Z.); yly@cslg.edu.cn (L.Y.)
[2] Key Laboratory of Special Purpose Equipment and Advanced Manufacturing Technology, Ministry of Education & Zhejiang Province, Zhejiang University of Technology, Hangzhou 310023, China; 1112102004@zjut.edu.cn (Y.X.); xuxuefeng@zjut.edu.cn (X.X.)
[3] School of Mechanical Engineering, Yanshan University, Qinhuangdao 066000, China
* Correspondence: daweijiju@163.com (J.G.); shuiquan.huang@ysu.edu.cn (S.H.)

Abstract: Grinding fluid often struggles to enter the grinding area and overcoming this challenge has been a major focus of research in recent years. Therefore, CNTs@T304 nano-capsules are prepared by filling the cavities of CNTs with a lubricant of T304. CNTs@T304 nano-capsules were used as an additive in this paper to prepare resin grinding wheels and nanofluids, respectively. The resin wheels filled with nano-capsules were used for grinding under the lubrication of nanofluids, and T304 could then be released to the grinding area to play a self-lubricating role during grinding. First, CNTs@T304 nano-capsules were characterized, and the properties of the prepared grinding wheels and nanofluids were tested. Second, the effects of the filling of nano-capsules and grinding speed on the grinding force, grinding temperature, surface roughness, and grinding ratio were studied. Finally, the lubrication mechanism of the nano-capsules was revealed through surface analysis of the workpiece. The results suggested that nano-capsules had good thermal stability and the nanofluid prepared from them exhibited good dispersion stability and thermal conductivity. The grinding wheel was found to satisfy the service conditions when the filling content was less than 15%. Compared with a common wheel, the grinding force and grinding temperature were reduced by 24% and 28%, respectively, and the surface roughness of the workpiece and the grinding ratio were increased by 18% and by 21%, respectively, when grinding GCr15 steel with the nano-capsule wheel. Lubrication with nanofluids could further reduce the grinding force, grinding temperature, and surface roughness values. During grinding, the self-lubrication film formed by the T304 released from the nano-capsules in the wheel served first and foremost as a lubricant. The intervention of the nanofluid enhanced the heat-exchange effect and lubrication efficiency in the grinding zone.

Keywords: CNTs; nano-capsules; nanofluids; grinding wheel; grinding; lubrication mechanism

check for updates

Citation: Guan, J.; Zhu, Z.; Yang, L.; Xia, Y.; Xu, X.; Huang, S. Synergistic Lubrication Mechanism of Nano-Fluid and Grinding Wheel Prepared by CNTs@T304 Nano-Capsules. *Lubricants* **2023**, *11*, 244. https://doi.org/10.3390/lubricants11060244

Received: 9 May 2023
Revised: 26 May 2023
Accepted: 30 May 2023
Published: 1 June 2023

1. Introduction

Grinding is characterized by a high precision and good surface quality and is the final process of general precision machining. The processing of brittle and hard materials is also mostly achieved through grinding. During grinding, the airflow formed by the high-speed rotation of the grinding wheel hinders the effective infiltration of the grinding fluid, preventing sufficient cooling and lubrication of the grinding zone and leading to various surface-quality problems [1–3]. At present, high-pressure injection and air baffle cut-off airflow methods are often used to enhance the cooling and lubrication efficiency of the grinding area [4,5], and other enhanced liquid-supply methods, such as minimum quantity lubrication (MQL) with nanofluids and direct lubrication of a self-lubricating grinding wheel, have also been studied [6,7]. Nanofluids are suspensions of nanoparticles, and nanoparticles can improve the heat-transfer performance and lubrication performance of the base fluid when used for MQL cutting/grinding. Shen et al. studied the performance

MoS_2 nanofluid when grinding cast iron under MQL conditions. When compared to the base oil, the experimental results showed that mustard oil, paraffin oil and soybean oil nanofluid with added MoS_2 nano-particles could reduce the grinding force by 27%, 21%, and 9%, respectively, and increased the service life of the grinding wheel by 46%, 35%, and 15% [8]. Li et al. prepared carbon nanotubes (CNTs)/MoS_2 mixed nanofluids and conducted experiments on grinding nickel alloys under MQL conditions, which revealed that the mixed nanofluids could produce a "physical synergistic effect", resulting in lower grinding forces and a better workpiece quality [9–11]. However, plain nanoparticles suffer from problems such as poor stability and easy sedimentation in nanofluids [12,13].

Scholars have developed self-lubrication grinding wheels that autonomously release lubricant during grinding, which can achieve enhanced lubrication. Shaji et al. prepared a resin grinding wheel using graphite as a filler, and the graphite was released into the grinding area to provide a good lubrication effect during the grinding process [14]. Yamaguchi et al. added microcapsules (5–20 μm) containing lubricants into the grinding wheel, and the lubricant could directly enter into the grinding area for lubrication during grinding with the damage of the microcapsules [15]. However, the relatively large size of the microcapsules at the micron level caused the lubricant inside the microcapsules to be thrown out when the grinding wheel rotated at high speed, resulting in insufficient lubrication during subsequent grinding. Xu et al. prepared self-lubricating resin grinding wheels using microcapsules of β-cyclodextrin/liquid lubricant as fillers, and the release of lubricant could act as a lubricant as the microcapsules broke during grinding [16]. However, the capsule filling has a great impact on the strength of the grinding wheel, and there is a risk of breakage when the grinding wheel rotates at high speed.

CNTs are nanotubes formed by curling flake graphite and have excellent thermal conductivity, mechanical properties, and lubrication properties [17,18]. The hollow structure allows guest molecules to enter their molecules to form nano-capsules, improving the performance of CNTs themselves [19,20]. To better lubricate the grinding area, our research group proposed to fill lubricant dibutyl phosphite (T304) into CNTs to prepare CNTs@T304 nano-capsules. Grinding wheels with self-lubricating properties were developed using nano-capsule as fillers, and the nano-capsule grinding wheels were applied to grinding under the lubrication of nanofluids prepared from nano-capsules. On the one hand, the nanofluid prepared by nano-capsules has better dispersion stability and lubrication properties compared with that prepared by commercially available CNTs without treatment, which can better enhance the cooling and lubrication performance. On the other hand, filling of CNTs@T304 nano-capsules can enhance the strength of the grinding wheel, achieving higher grinding speeds, and the nano-capsules can also evenly release T304 for lubrication during the grinding process. The goal of this research is to develop a practical nano-capsule grinding wheel and nanofluid and to study their synergistic self-lubricating mechanism during grinding. This research lays a theoretical foundation for the application of new nano-capsule grinding wheels and nanofluids in MQL.

2. Materials and Methods

2.1. Preparation and Characterization of CNTs@T304 Nano-Capsules

Commercial CNTs were sourced from Shanghai Aladdin Company, with a purity of ≥95.5% and an inner cavity diameter of about 15 nm. T304 was provided by Jinzhou Kangtai Chemical Company. The purchased CNTs had a relatively large length and diameter, making them less conducive to filling. Therefore, it was necessary to first shorten and pre-treat the CNTs [21]. During the treatment, 50 g of CNTs were added to 1500 mL of 40% concentrated nitric acid, and the mixture was loaded into a three-necked flask. After heating and refluxing at 80 °C for 8 h, magnetic stirring was applied at a rotation speed of 500 r/min. Finally, the mixture was subjected to vacuum filtration, and the resulting filter cake was dried at 85 °C and ball milled for 10 h to obtain acidified CNTs. In the preparation of CNTs@T304 nano-capsules, 20 g of T304 was first dissolved into 1000 mL of acetone, and 40 g of acidified CNTs was added. The two were mixed thoroughly, placed in a spherical flask, and evacuated to −0.2 MPa. The mixture was shaken with ultrasound at 70 °C for 5 h. After ultrasound, the mixture was filtered again. During filtration, the filter cake was washed with acetone to clean any T304 molecules that had not yet been filled. Finally, the filter cake was placed in an oven and dried at 80 °C for 8 h, followed by ultrafine particle grinding to obtain nano-capsules. The sample structure was observed using an FEI TECNAI G20 transmission electron microscope (TEM) with an accelerated voltage of 200 KV during observation. Thermogravimetric analysis was performed on a STA449 thermal analyzer with a temperature rise range of 20–800 °C and a rate of 20 °C/min.

2.2. Preparation of Nanofluids and Nano-Capsule Grinding Wheels

A surfactant can significantly reduce the surface tension of the base solution, which should be added into the water solvent to improve the dispersion and concentration of nano-capsules in the nanofluid [22], although it may have a certain corrosive effect on the surface of the workpiece. Through preliminary experiments, a mixture of the nonionic surfactant Tween-80 (TW-80) and the anionic surfactant sodium dodecyl benzene sulfonate (SDBS) (mass ratio 7:3) was selected as a composite surface dispersant. The formula of the water-based nanofluid samples can be seen in Table 1. After the mixing of the components was completed, the mixture was mechanically stirred at 50 °C for 30 min and subjected to 1 h of ultrasonic dispersion to prepare a grinding nanofluid, as shown in Figure 1a. After the preparation was completed, the dispersion stability, heat-transfer performance, and wetting performance of the nanofluid were tested: (1) To test the dispersion stability, the nanofluids containing 0.1–1.2 wt.% nanoparticles were left for 30 days, and 1 mL of the upper liquid was taken daily and diluted twice before being placed in a colorimetric dish. The absorbance of the nanofluid at a wavelength of 500 nm was measured using a 752N ultraviolet visible spectrophotometer at a temperature of 20 °C, and the stable absorbance value was used as the basis for determining the dispersion stability of the nanofluid [23]. (2) For the heat-transfer performance test, the thermal conductivity of each group of samples was measured using a TC3010L thermal-conductivity meter, with each injection of about 30 mL. After the injection was completed, the thermal conductivity was automatically measured by the instrument. (3) The wettability of the nanofluid was evaluated based on its contact angle on the surface of 45# steel. The contact angle was measured using the Kruss DSA25 contact-angle-measuring instrument, with a sample injection rate of 2 μL drops per test. After approximately 15 s of steady contact with the 45# steel surface [24], the sample stage was moved to keep the droplets in optimum display and readings were taken.

When preparing nanoparticle-filled grinding wheels, 15% phenolic resin powder, 0–20% commercial CNTs or nano-capsules, and 85–55% 220# white alumina were mechanically stirred evenly in proportion (CNTs or nano-capsules were set with a mass fraction increasing by 2%), and then placed in a ball mill for 6 h. During stirring, an appropriate amount of furfuryl alcohol was added as a wetting agent (with the formula given in Table 2). The raw materials were then placed into a splayed cavity mold and an annular mold, respectively. The mixture was then pressed at 60 MPa for 10 min, and the samples were removed and placed in an oven to cure for 12 h at a curing temperature of 160 °C and a rise rate of 10 °C/h [25]. Finally, a circular wheel specimen of D175 mm × d80 mm × H27 mm was made after free cooling for grinding performance testing, as shown in Figure 1b. A D80 mm × h20 mm "8-shaped" block specimen was used for mechanical performance testing, as shown in Figure 1c. During strength testing, tensile strength testing was carried out on the RG 4100 universal material-testing machine with a tensile rate of 0.5 mm/min. The testing machine automatically loaded the tensile force and recorded the tensile strength. During hardness testing, the hardness of the abrasive was measured using an HR-150A Rockwell hardness tester with a hardness tester indenter of 3.175 mm diameter, a preload force of 98 N, and a main load of 588 N [26]. The measurements were taken at 4 points from the center of the circle on both sides to 1/2 of the outer circle and the average of each measurement was taken.

Table 1. Sample formula of grinding nanofluid.

Composition	Content	Function
Deionized water	97.3–98.4 wt.%	Base fluid
CNTs or nano-capsules	0.1–1.2 wt.%	Lubricating additive
TW-80/SDBS	0.5 wt.%	Active agent
Triethanolamine	0.5 wt.%	Rust inhibitor
Sodium benzoate	0.5 wt.%	Antiseptic

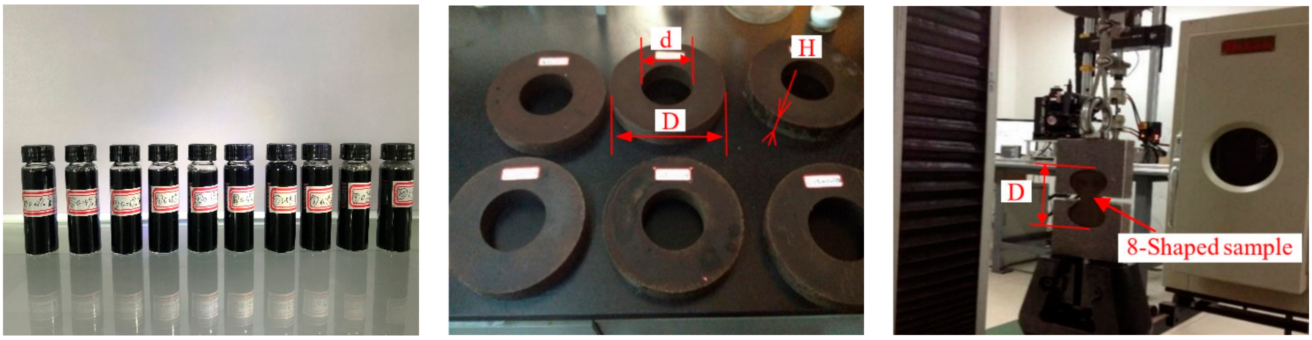

(**a**) (**b**) (**c**)

Figure 1. The prepared nanofluid (**a**), grinding wheel (**b**), and tensile strength test (**c**).

Table 2. Formula of self-lubricating grinding wheels.

No.	Resin	Abrasive	CNTs	CNTs@T304 Nano-Capsules
A0 (Common Wheel)	15 wt.%	85 wt.%	—	—
B2-B20 (CNT Wheel)	15 wt.%	83–65 wt.%	2–20 wt.%	—
C2-C20 (NC Wheel)	15 wt.%	83–65 wt.%	—	2–20 wt.%

2.3. Grinding Test Scheme

The grinding experiment was conducted on the M7140 precision surface grinding machine with variable frequency and speed regulation. Before the grinding experiment, the grinding wheel needed to be accurately dynamically balanced. Five more adjustments with a diamond pen were also required, with a grinding speed of 17.8 m/s and a single-pass adjustment of 0.2 mm. The experimental conditions are shown in Table 3, and the GCr15 steel (C: 0.95–1.05, Cr: 1.40–1.65 Mn: 0.25–0.45, Si: 0.15–0.35, Mo: $\leq$0.10, Ni: $\leq$0.30, S: $\leq$0.025, P: $\leq$0.025) was supplied by Longteng Special Steel Co., Ltd. The experimental plan was as follows. First, the grinding speed was fixed at a grinding speed of 17.8 m/s, and a grinding wheel with CNTs or nano-capsule mass fractions of 2–20% was applied to grind under MQL conditions of commercially available emulsions, CNT nanofluids, and nano-capsule nanofluids. Compared with common wheels without fillers, the influence of changes in the nano-capsule content on the grinding force, grinding temperature, surface quality, and grinding ratio was studied. Second, wheels with a mass fraction of CNTs or nano-capsules of 14 wt.% were selected to grind at a grinding speed of 17.8 m/s, and MQL grinding was conducted using nanofluids with a concentration of 0.1–1.2 wt.%. Finally, the effect of the grinding speed on the grinding performance was tested using grinding wheels with CNTs or nano-capsules with a mass fraction of 14 wt.%, with the grinding speed varying between 4.45 and 26.7 m/s, compared to common grinding wheels; three parallel experiments were conducted for each group of experiments.

Table 3. Experimental conditions for grinding test.

Machine Tool	Grinding Wheel	Workpiece	Cooling Conditions	Grinding Speed (m/s)	Feed Speed (m/s)	Grinding Depth (μm)	Total Grinding Depth (μm)
M7140	2–20 wt.% wheel	GCr15 steel (HRC60-62), 100 × 50 × 50 mm	Nanofluid under MQL, 50 mL/min	4.45, 8.9, 13.35, 17.8, 22.25, 26.7	0.2	10	300

During grinding, the normal grinding force (F_n) and tangential force (F_t) were measured using a Kistler 9129A dynamometer and the combined force of the two cutting forces was used as the cutting force evaluation standard [27,28], as shown in Figure 2a. During the grinding process, thermocouples were adopted to measure the grinding temperature. K-type thermocouples were buried in a pre-machined temperature-measurement hole, which was approximately 1.5 mm away from the upper surface [29,30], as shown in Figure 2b. A dial indicator was applied to measure the wear of the wheel, and the TR-200 surface roughness meter was used to test the surface roughness of the workpiece.

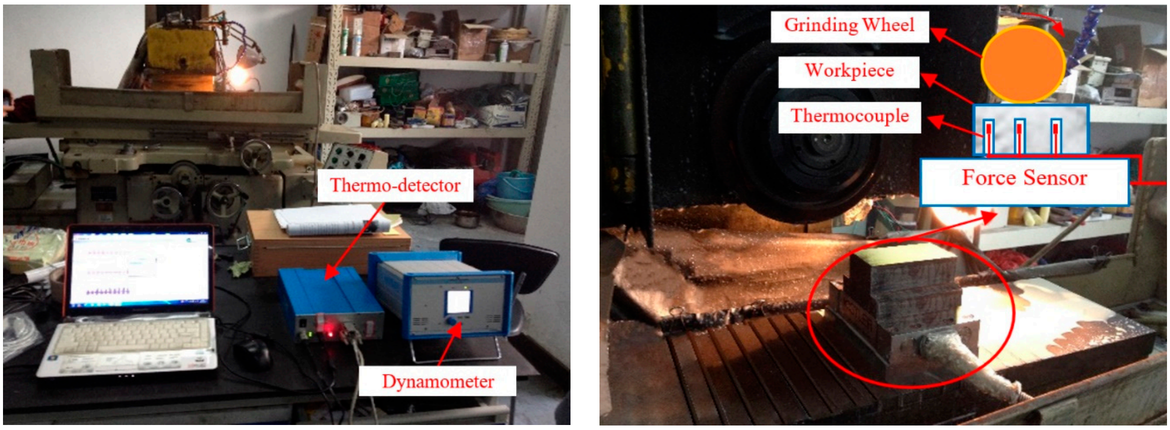

(**a**) (**b**)

Figure 2. The grinding equipment (**a**) and the grinding force tester (**b**).

To study the lubrication mechanism of the nano-capsule grinding wheel and nanofluids, a 100 mm × 45 mm × 0.8 mm GCr15 steel plate was fixed on a steel piece for grinding. The steel sheet was then taken down and ultrasonically cleaned in acetone for 20 min, and an AXISUltra DLD X-ray photoelectron spectrometer (XPS) was used to detect the binding energy of the elements on the surface. During the test, the electronic energy was 80 eV and the binding energy of the carbon C_{1s} was 284.8 eV as the internal standard [31].

3. Experimental Results

3.1. Characterization of Nano-Capsules

Figure 3 presents TEM images of the nano-capsules. It can be seen that several segments of the cavity of CNTs are filled with other substances, which should be T304, indicating that T304 is filled into the CNTs and forms nano-capsules. Capillary action is the main driving force for other liquid substances to be filled into the cavity of CNTs, but it is premised on sufficient force between the filled substance and the pipe wall to induce wetting at the interface [32]. Moreover, the contact angle θ of the liquid determines whether CNTs can be wetted by liquid and undergo capillary action. When $\theta > 90°$, the pressure difference ΔP at the gas–liquid interface is negative and infiltration cannot occur. When $\theta < 90°$, the infiltration phenomenon occurs and the filling effect can only proceed. Therefore, only substances with small contact angles and surface tension below 200 mN/m, such as ethanol, acids, etc., can be filled into CNTs under specific conditions. In the present study, the surface tension of T304 was about 40 mN/m, and after it was dissolved in acetone, the surface tension was further reduced, making it easier to enter the CNTs through capillary action. Subsequent drying caused the acetone to evaporate, while the T304 was retained in the tubes.

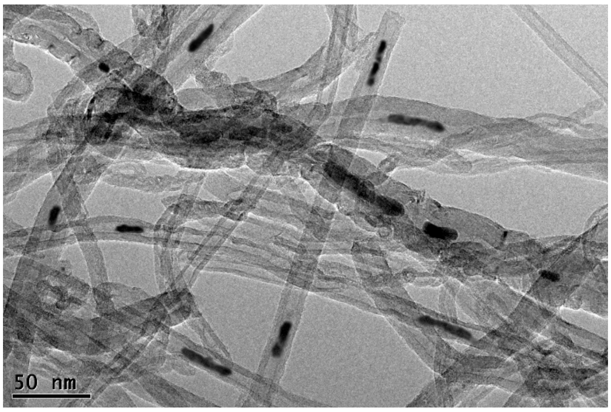

Figure 3. TEM image of CNTs@T304 nano-capsules.

Figure 4a,b show the thermogravimetric (TG) analysis and differential thermal analysis (DSC) results, respectively, of acidified CNTs, T304, and CNTs@T304 nano-capsules. In Figure 4a, the nano-capsules underwent a weight-loss process at around 200 °C, while acid-treated CNTs did not exhibit a similar process, indicating the escape of T304 from the nano-capsules after heating. The filling rate of T304 in nano-capsules (η) can be calculated based on the latent heat of phase change Formula (1) [33]:

$$\eta = H_f / H_p \times 100\% \quad (1)$$

where H_f is the phase-change latent heat of T304 in the nano-capsules and H_p refers to the phase-change latent heat of T304 of the same mass, in J/g. In Figure 4b, both T304 and nano-capsules had a low-temperature phase-change endothermic process, and the phase-change latent heat value in this process could be calculated from the peak area enclosed by the DSC curve and baseline. By plotting and calculating, it could be obtained that the phase-transition latent heat of T304 in the nano-capsules was about 35.2 J/g and the phase-transition latent heat of the same mass of T304 was about 178.4 J/g. The filling rate of T304 was calculated to be about 20%.

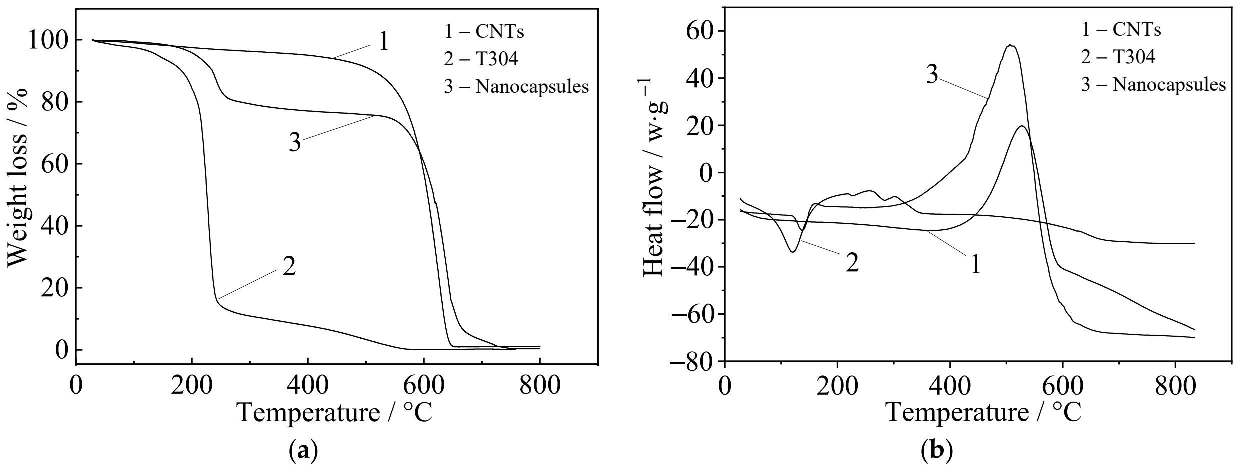

Figure 4. TG (**a**) and DSC (**b**) curves of CNTs, T304, and nano-capsules.

3.2. Performance Testing of Nanofluid and Nano-Capsule Grinding Wheels

Figure 5 shows how well the concentration of acidified CNTs or nano-capsules affects the absorbance of nanofluid, and the error bar in Figure 5 is used to represent the error range of a group of experiments. The following are all the same meanings. It can be seen that when the concentration was low, the absorbance would gradually increase with the increase in concentration, and there was a certain linear relationship. When the concentration of nanoparticles reached a "saturation" concentration (about 0.5%), the increase in absorbance was not significant, which was due to the sedimentation of some nanoparticles that had not been effectively dispersed. The superior dispersion stability of the nano-capsules over the acidified CNTs at the same concentrations could be attributed to the partially exposed oleic acid molecular groups outside the CNTs, which can combine with surfactants and further enhance the dispersion effect.

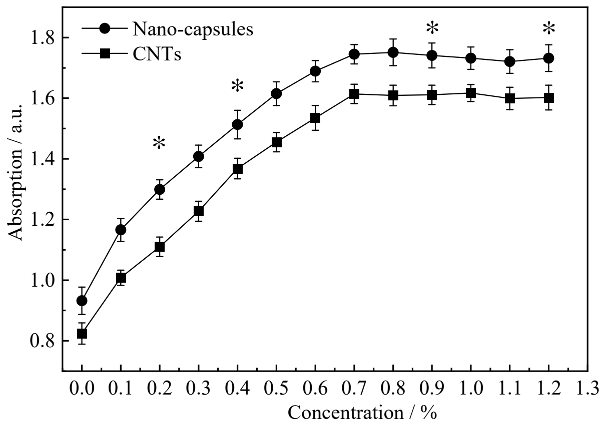

Figure 5. Influence of nanoparticle concentration on the absorbance of nanofluid (* $p \leq 0.05$).

CNTs are good heat conductors and can significantly improve the heat-transfer performance of liquids. The application of CNTs to enhance the heat transfer in grinding fluids is of good value [34,35]. Figure 6a shows the influence of the concentration of nanoparticles on the thermal conductivity. It can be observed from the results that when the content was low, the thermal conductivity would increase with an increase in the concentration. The nano-capsules could increase the thermal conductivity of the base liquid by up to 110%. When the concentration continued to increase, the increasing trend of the thermal conductivity would slow down, which was due to the agglomeration and sedimentation of excess nanoparticles, resulting in a reduction in the heat-transfer effect [36,37].

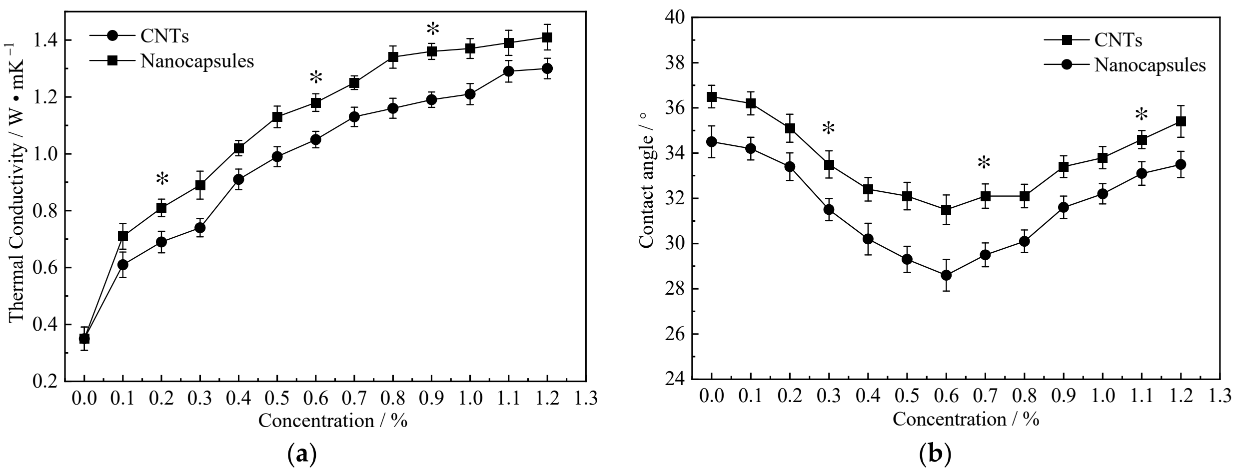

Figure 6. Influence of nanoparticle concentration on thermal conductivity (**a**) and contact angle of nanofluid (**b**) (* $p \leq 0.05$).

Figure 6b presents the influence of the content change of nanoparticles on the wettability of nanofluids when the surfactant concentration was 0.5%. It can be observed that when the concentration of nanoparticles increased, the contact angle of the nanofluid decreased first and then increased. The analysis indicates that CNTs may have certain surface activity after acid treatment. After complete dispersion in the base liquid, the repulsion between nanoparticles and the base fluid molecules increased the molecular spacing on the free surface and acted to reduce the surface tension [38,39]. If the concentration of nanoparticles was too high, the dispersion stability of the nanofluid was poor, which led to an increase in the intermolecular force and viscosity, resulting in an increase in the contact angle. In addition, the thermal conductivity and wetting performance of the nano-capsule nanofluid were superior to those achieved with commercial CNTs at various concentrations. This was because the nano-capsules had a stronger surface activity, more uniform dispersion, and better stability in the base liquid [40,41]. Nanofluids with better thermal conductivity and wetting properties can perform better heat transfer and permeation in the grinding area.

Figure 7 presents the effect of different contents of CNTs or nano-capsules on the tensile strength and hardness. In Figure 7a, it can be seen that as the content increased, the tensile strength exhibited a trend of first increasing and then decreasing. This is because the surface activity of CNT particles is high and a large number of unsaturated residual bonds and active groups on their surface cause them to undergo physical or chemical crosslinking with resin, enhancing the bonding force at the material interface. Continuous addition of CNTs may lead to problems with their aggregation, which reduces the cross-linking effect and the binding strength. The optimal content of nanoparticles was about 5%, and when the filling content was about 10%, the strength of the nano-capsule wheel was comparable to that of a common wheel. The filling of nano-capsules had a more significant enhancement effect on the strength and hardness due to the smaller aspect ratios of the nano-capsules and the closer binding effect with the resin. As shown in Figure 7b, the hardness of the wheel decreased with the increase in the content of the filler. When the content of the nano-capsules was 16%, their tensile strength was about 8.2 MPa and their hardness was 52 HRE. Therefore, when the content was less than 16%, the conditions for applications could still be met [42].

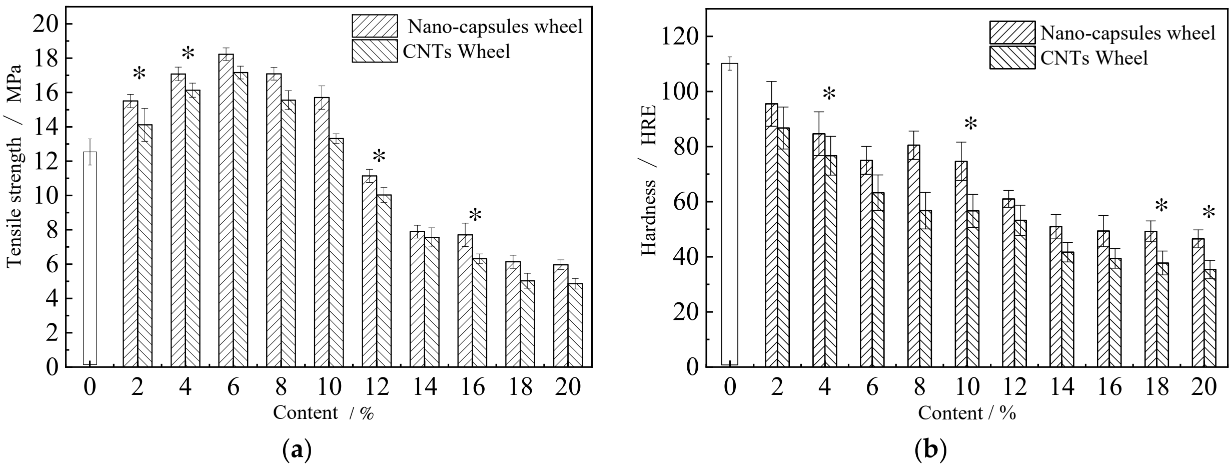

Figure 7. Effect of content of CNTs and nano-capsules on tensile strength (**a**) and hardness (**b**) of grinding wheels (* $p \leq 0.05$).

CNTs@T304 nano-capsules may be damaged during the curing process. Therefore, it is necessary for the nano-capsules to have certain stability and compatibility with the resin during curing. From the thermal weight-loss curve of the nano-capsules in Figure 4a, it can be observed that significant weight loss occurred only at temperatures above 200 °C, which is sufficient to resist the curing temperature (160 °C). Figure 8a shows the infrared spectra of the solidified tissues of the wheel. The peaks of 1628 cm^{-1}, 2583 cm^{-1}, 2924 cm^{-1}, and 3424 cm^{-1} in the nano-capsule spectra represented the absorption peaks of skeleton vibration, C-H stretching vibration, C-H deformation vibration, and O-H bond stretching vibration, respectively [43]. The first three peaks were present in the spectrum of the wheel, indicating that the skeleton structure of CNTs was not destroyed during the curing process, which provided sufficient protection for the internal T304. Figure 8b shows an SEM image of tissues of the wheel, which indicated that nano-capsules were distributed in the form of clustered particles, with each particle acting as an oily capsule.

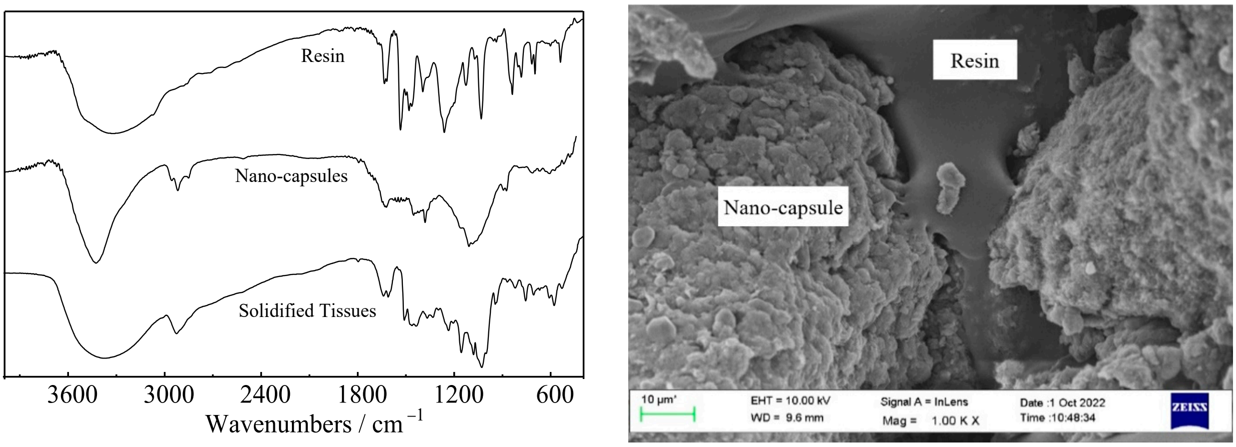

(**a**) (**b**)

Figure 8. FTIR (**a**) and SEM (**b**) analysis of wheel structure.

3.3. Grinding Force and Grinding Temperature

Figure 9a,b show the changes in grinding force and temperature, respectively, of a wheel filled with CNTs or nano-capsules under MQL conditions of commercially available emulsions, 0.5 wt.% CNT nanofluid, or nano-capsule nanofluid, respectively. It can be seen that as the content of CNTs increased, the grinding force and grinding temperature during the processing of CNT wheels first decreased and then slowed down. This is because the structure of the CNTs was destroyed as the wheel wore during grinding, and the carbon deposition film formed could play a certain role in reducing friction. However, the release of excessive CNTs may hinder friction, resulting in little change in the grinding force and temperature. The grinding force and temperature also decreased with the increase in the content of the nano-capsules. When the nano-capsule content exceeded 12%, the change in the grinding force and temperature was not significant. In addition, the grinding forces or temperatures of the nano-capsule wheels were lower than those of CNT wheels under different content. This was because the nano-capsules in wheels were damaged during the grinding process and released T304, which forms a lubricating film in the grinding area together with the friction products of CNTs, further reducing the grinding force and temperature. The optimal content of nano-capsules in grinding wheels was about 12%, which could reduce the grinding force by an average of about 45% and the grinding temperature by about 35% compared to common wheels. In Figure 9, when the same type of grinding wheel was lubricated with different grinding fluids, nano-capsule nanofluids presented the best effect on reducing the grinding force or temperature, followed by CNT nanofluids, and commercially available emulsions had the worst effect.

Figure 10 shows the influence of the nanoparticle concentration of nanofluids on the grinding force and temperature when grinding with CNT or nano-capsule wheels with a filler content of 10 wt.%. It can be observed that, with the increase in concentration, the grinding force or grinding temperature showed a trend of first decreasing and then slowly increasing. When the concentration of CNTs was about 0.6 wt.%, the minimum grinding force and grinding temperature could be obtained. When the concentration of nanoparticles was low, fewer nanoparticles acted on the grinding zone and the grinding fluid failed to exert lubrication and heat-exchange effects better, so the anti-friction and cooling effect on the grinding zone was limited. When the concentration of nanoparticles was high, the dispersion of nanoparticles in the base fluid was unstable and the nanoparticles would appear to exhibit agglomeration, leading to a reduction in the nanoparticles actually entering the grinding area, leading to increased friction. Under different concentrations, the nanofluids prepared with nano-capsules exhibited better lubrication effects. This is because nano-capsules have better dispersion stability in the base fluid and the prepared nanofluids are more uniform and consistent, making it easier to penetrate into the grinding area.

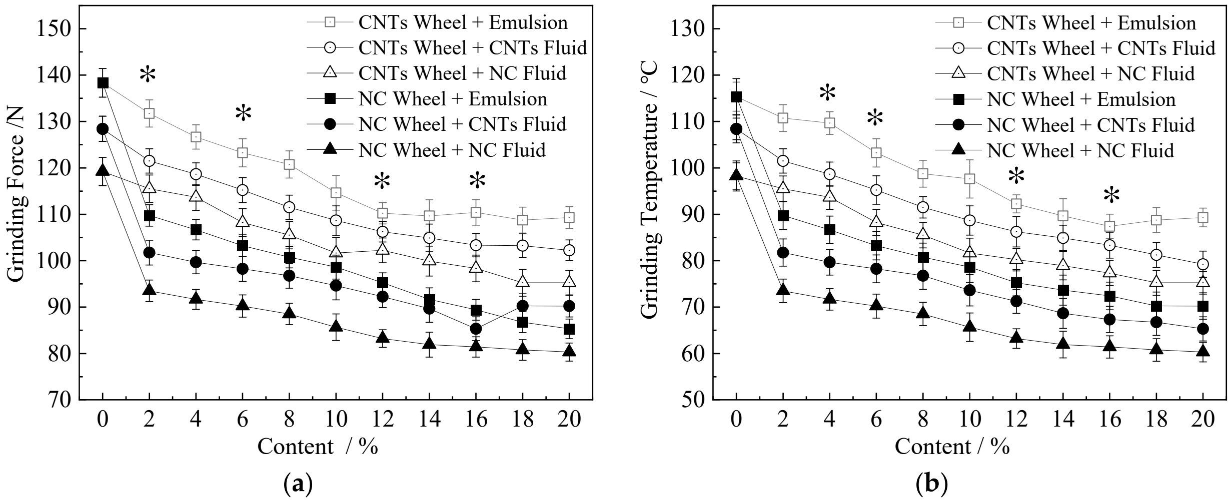

Figure 9. Influence of filler content of wheels on grinding force (**a**) and grinding temperature (**b**) (* $p \leq 0.05$).

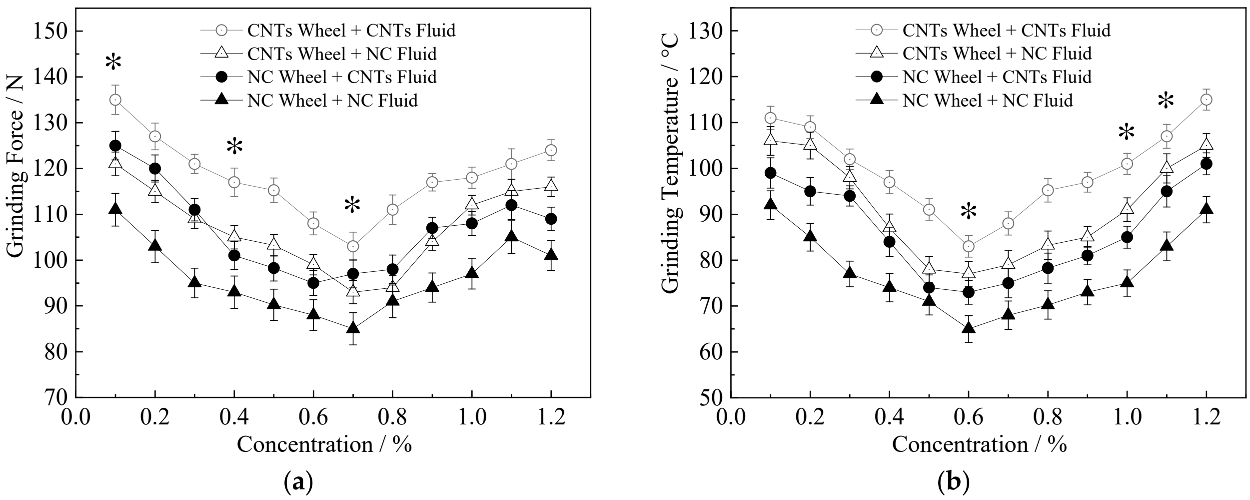

Figure 10. Influence of concentration of nanoparticles in nanofluid on grinding force (**a**) and grinding temperature (**b**) (* $p \leq 0.05$).

3.4. Grinding Ratio and Workpiece Surface Roughness

The grinding ratio is the volume ratio of the removed metal to the wear of the grinding wheel [44]. Figure 11a reveals the relationship between the grinding ratio and the change in filler content. Due to the high hardness of GCr15 steel and the poor retention of resin binder on abrasive particles, the grinding ratio of the wheel in this experiment was small but within the normal range. As indicated in Figure 11a, the grinding ratios of CNT wheels and nano-capsule wheels appeared to increase and then decrease as the filler content increased. The highest values of the grinding ratio were 10% and 12%, respectively. When less filler was added, due to the self-lubricating effect of the filler, the grinding ratio could be improved. When the filler content was high, the hardness of the grinding wheel decreased and the microstructure of the wheel became soft, resulting in a decrease in the grinding ratio. Under the same experimental conditions, the grinding performance of nano-capsule grinding wheels was about 35% higher than that of common grinding wheels on average, and 25% higher than that of CNT wheels. When the same type of grinding wheel was lubricated with different nanofluids, nano-capsule nanofluids exhibited the best effect on improving the grinding ratio, followed by CNT nanofluids, and commercially available emulsions had the worst effect.

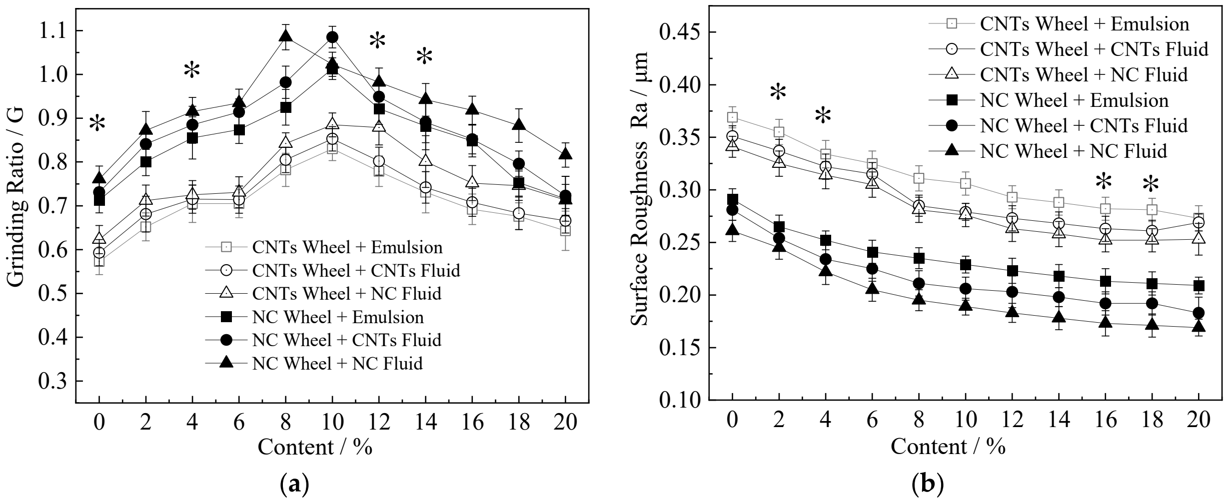

Figure 11. Influence of filler content of wheels on grinding ratio (**a**) and surface roughness (**b**) (* $p \leq 0.05$).

Figure 11b shows the variation in the surface roughness of the workpiece after grinding with different grinding wheels. The surface roughness values of workpieces ground with CNT wheels or nano-capsule wheels decreased by approximately 10% and 15%, respectively, compared to those ground with common wheels. For nano-capsule wheels, the surface roughness of the workpiece tended to decrease with the increase in filling content. The surface roughness of the workpiece is not only determined by the precision of the machine tool and grinding wheel, but also influenced by the detachment of abrasive particles. When grinding with common wheels, high grinding temperatures, high grinding forces, and strong abrasive wear effect led to poor surface roughness of the workpiece. Grinding wheels filled with nano-capsules could directly and effectively provide lubrication during grinding, reducing abrasive wear, thereby reducing the grinding force and temperature and improving the surface quality of the workpiece. In addition, due to the large pores of the grinding wheels, grinding debris fills the pores and can cause further scratches on the workpiece during the grinding process. However, for nano-capsule wheels, the self-lubrication film formed can prevent the grinding debris from entering and causing scratches on the workpiece, thereby improving the surface quality of the workpiece.

Figure 12 shows the effect of the content of CNTs or nano-capsules on the grinding ratio and workpiece surface roughness. It can be seen that with an increase in the nanoparticle content, the grinding ratio exhibited a certain trend of first increasing and then decreasing, while the workpiece surface roughness showed a trend of first decreasing and then increasing. When the content of additives was about 0.6%, the effect of the nanofluid on improving the grinding ratio and reducing the workpiece surface roughness was more obvious. This is because when the content of nanoparticles is low, there are fewer nanoparticles entering the grinding area, which has a limited lubrication and polishing effect. When the content is excessively high, it will lead to the agglomeration and precipitation of nanoparticles, which will result in fewer nanoparticles entering the grinding area, causing insufficient lubrication in the grinding area, the deterioration of the workpiece surface quality, and the intensification of grinding-wheel wear. Nanofluids prepared from nano-capsules were more effective in reducing the surface roughness than nanofluids prepared from acidified CNTs. First, nano-capsules nanofluids more easily penetrate into the grinding area, and more nanoparticles play an effective role. In addition, the molecular structure of nano-capsules is destroyed during grinding, and T304 is released in the grinding area, forming a more sufficient and complex lubrication film, which gives the nanofluids prepared by nano-capsules a better lubrication effect [45].

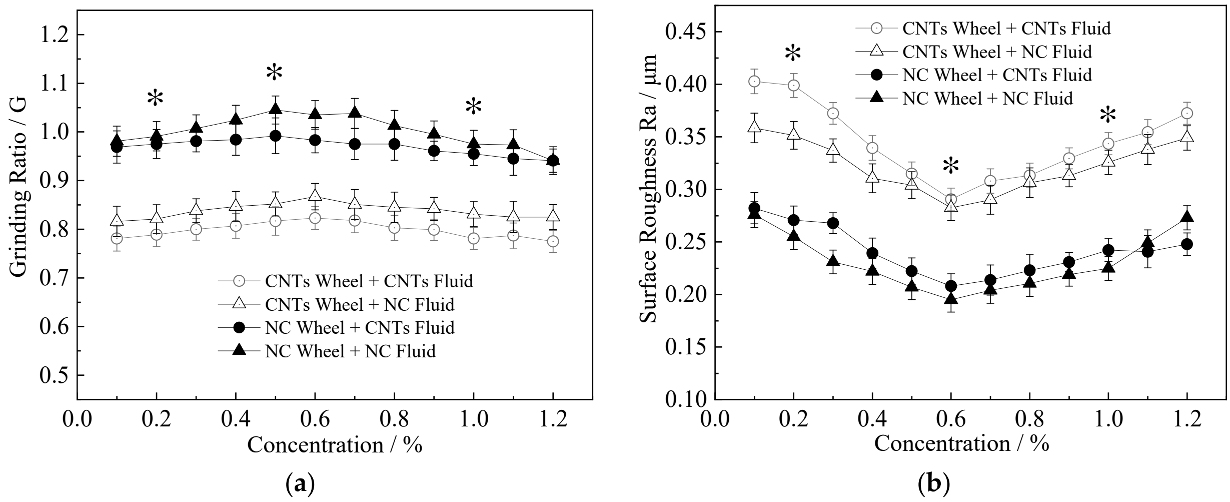

Figure 12. Influence of concentration of nanoparticles in nanofluid on grinding ratio (**a**) and surface roughness (**b**) (* $p \leq 0.05$).

3.5. Effect of Grinding Speed on Grinding Performance

The influence of the change in grinding speed on the grinding force is shown in Figure 13a. As can be seen, when other conditions remained unchanged, the grinding force of different wheels decreased with the increase in speed. Under the same mass fraction, the grinding force of CNT wheels was smaller than that of common wheels, while the grinding force of nano-capsule wheels was the smallest. The impact of changes in the grinding speed on the grinding temperature is shown in Figure 13b. It can be seen that under the condition that other processing parameters remained unchanged, the grinding temperature increased with the increase in the grinding speed. This is because as the speed increases, the number of abrasive particles involved in grinding per unit time increases, which intensifies the friction between the workpiece and the abrasive particles and results in an increase in the grinding temperature. Under the same content, the grinding temperature of CNT wheels was lower than that of common wheels, and the grinding temperature of nano-capsule wheels is also the smallest, indicating that nano-capsule wheels are more effective in reducing the temperature.

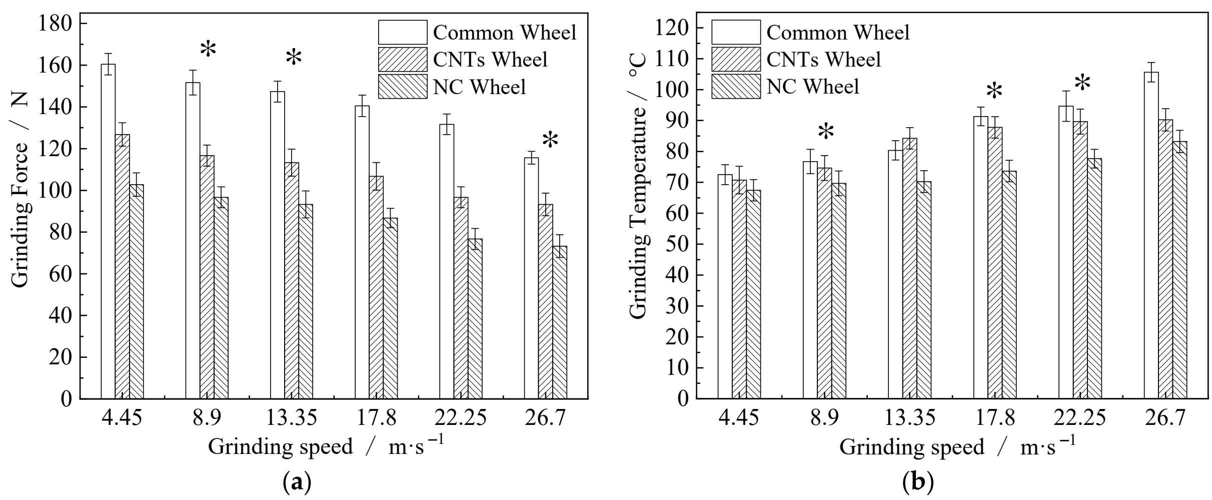

Figure 13. Influence of grinding speed of wheels on grinding force (**a**) and grinding temperature (**b**) (* $p \leq 0.05$).

In Figure 14a, the grinding ratio of the nano-capsule wheel was also the highest at different grinding speeds. This is caused by the fact that during grinding, T304 is released into the grinding area, forming a lubricating film between the abrasive particles and the surface of the workpiece, which exerts a certain amount of lubrication. In addition, the frictional state between the abrasive particles and the workpiece was improved due to the CNT friction products, leading to a reduction in the grinding force and temperature, resulting in lighter wear of the nano-capsule wheels. Moreover, due to the presence of a self-lubrication film, it was not easy to cause chips sticking to the surface of the wheel, as well as the resulting passivation of the wheel. The formation of a self-lubrication film avoids the adhesion between abrasive particles and chips, reduces the adhesion, blockage, and wear of the grinding wheel, and thus maintains the sharp cutting effect of the grinding wheel. From Figure 14b, it can be observed that the surface roughness of the workpiece decreased with the increase of the grinding speed. This is because the wheel is a multi-blade tool, and the faster the speed, the more surface blades participate in cutting per unit time, and the lower the thickness of each blade, resulting in a smaller surface roughness.

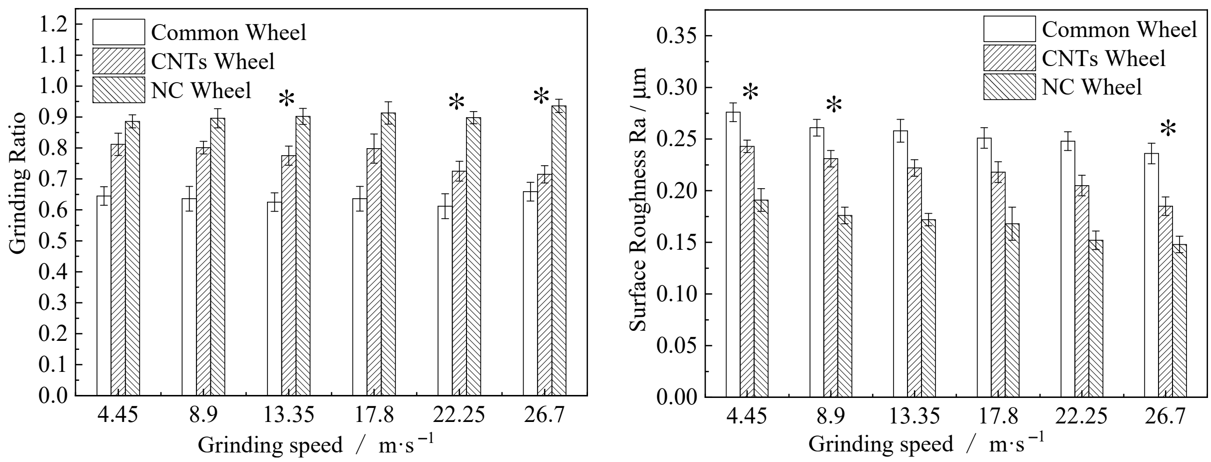

(**a**) (**b**)

Figure 14. Influence of grinding speed of wheels on grinding ratio (**a**) and surface roughness (**b**) (* $p \leq 0.05$).

4. Discussion of Lubrication Mechanism

Figure 15 shows SEM images of the workpiece after grinding with different grinding wheels. It can be seen that the surface ground with common wheels was relatively rough, and there were many deposits on it, which might be a transfer film formed by phenolic resin [46]. The workpiece ground with CNT wheels was relatively smooth with less sediment on it, while the surface was the smoothest when ground with nano-capsule wheels.

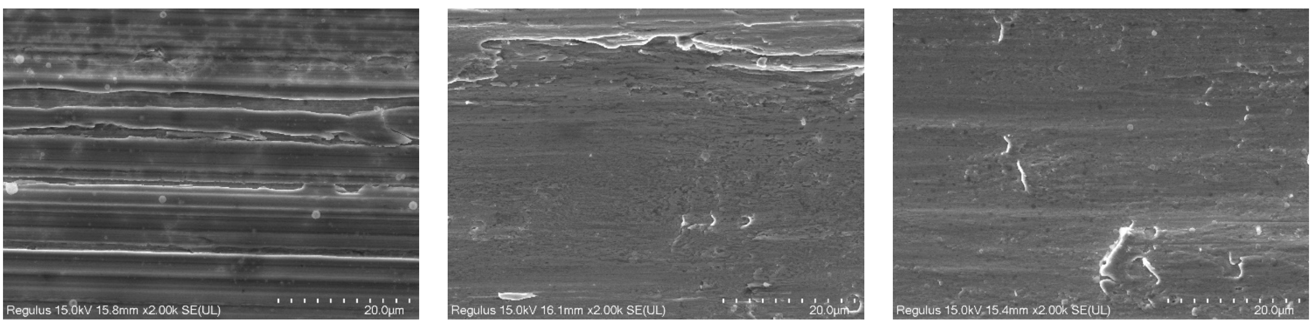

(**a**) (**b**) (**c**)

Figure 15. SEM morphology of workpiece surface ground with common wheel (**a**), CNT wheel (**b**), and nano-capsule wheel (**c**).

To demonstrate the release process of T304 and the formation of a self-lubricating layer on the surface of the workpiece during grinding, XPS energy spectrum analysis was conducted on the main elements on the surface of the workpiece ground with different wheels under MQL conditions of nanofluids. Figure 16 shows the XPS spectra of C, O, and P elements on surfaces ground with different grinding wheels. The XPSPEAK 41 software was adopted to divide the peaks of the elements, and the fitted peaks and possible corresponding groups were labeled in the graph. The relative atomic concentrations of the elements are listed in Table 4. It can be seen that the peak shapes of the C_{1s} and O_{1s} energy spectra on the surface of common wheels had a relatively homogeneous peak shape and mainly belonged to the resin fragments adsorbed on the metal surface and the types of elements in the iron oxide. This is because during the grinding process, the phenolic resin fractures and falls off, and some of the fragments formed are carbonized and deposited on the surface of the workpiece through adhesion.

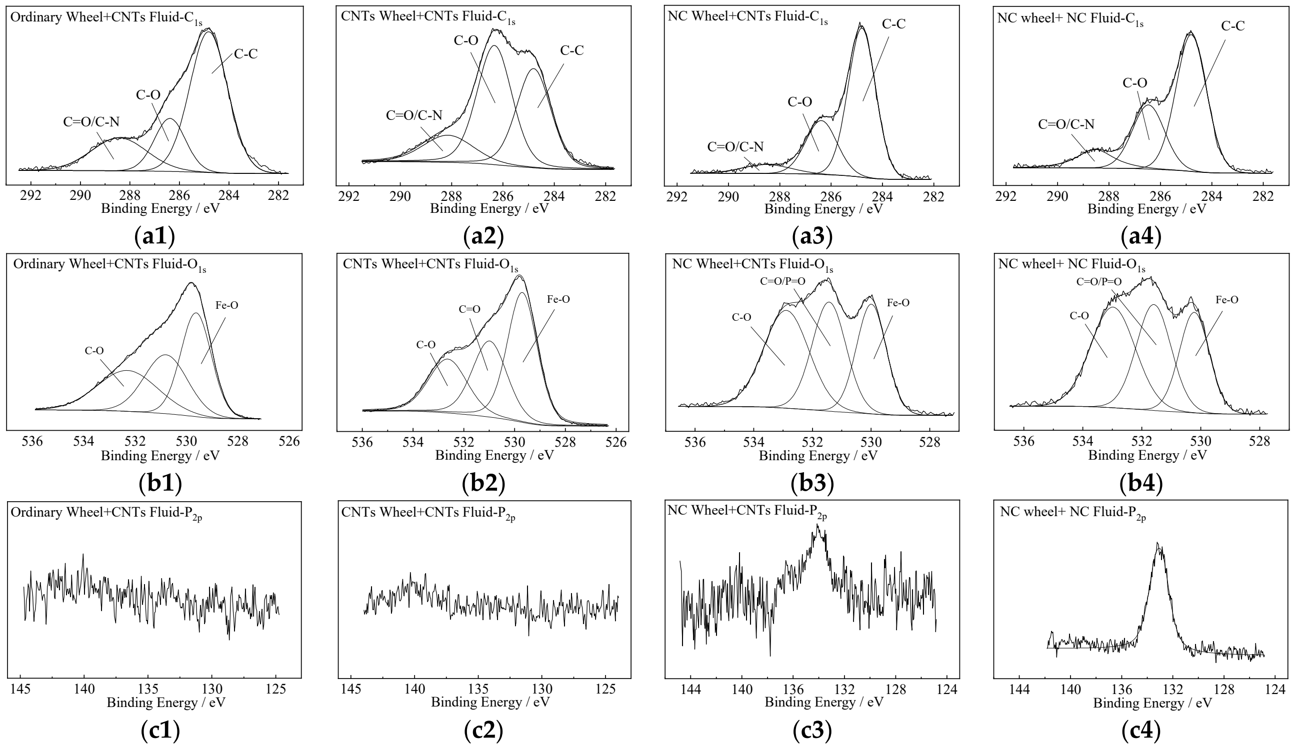

Figure 16. XPS energy spectra of C (**a1**–**a4**), O (**b1**–**b4**), and P (**c1**–**c4**) on the workpiece ground by common wheel, wheel filled with CNTs, and wheel filled with nano-capsules under the lubrication of CNT nanofluid and nano-capsule nanofluid.

Table 4. Relative atomic concentrations of the main elements on the workpiece surface ground with different wheels.

Type of Steel Surface	Relative Content/%			
	C	O	Fe	P
Common Wheel + CNT Fluid	20.31	35.13	44.56	—
CNT Wheel + CNT Fluid	30.17	29.76	40.07	—
NC Wheel + CNT Fluid	25.18	28.33	44.51	1.95
NC wheel + NC Fluid	27.86	32.71	37.05	2.38

In Figure 16(a2), compared to the surface of the workpiece ground with common wheels, the proportion of fitting peaks representing C-N groups in the C_{1s} spectrum on the workpiece surface ground with CNT wheels decreased, while the proportion of fitting peaks representing C/C-C groups increased. In Figure 16(b2), the proportion of fitting peaks representing C-O groups also decreased, indicating that the involvement of CNTs in grinding led to a reduction in the adhesion of the resin on the surface [47]. In Table 4, the relative atomic concentration of C_{1s} on the workpiece surface ground with a CNT grinding wheel was 16% higher than that of common wheel. This is because CNTs in the grinding-wheel structure participate in the grinding process, reducing the adhesion of resin fragments. CNTs themselves may also adsorb to the surface of the workpiece, forming different lubrication layers. The molecular structure of CNTs was destroyed during grinding, and the formed fragments could be deposited or adsorbed on the workpiece surface, exerting an anti-friction effect. However, the polarity of hydroxyl groups in the CNT molecules was weak and they could not be effectively and firmly adsorbed on the surface of the workpiece, so the self-lubricating effect of CNT grinding wheels was not significant [48].

In Figure 16(a3,b3), there are new peaks in the spectra of C_{1s} and O_{1s} on the surface of the workpiece ground with the nano-capsule wheels. Among them, the binding energy of about 288.8 eV and 533.8 eV should be attributed to the carbon and oxygen types in C=O, respectively [49,50], and the presence of carboxyl groups in the molecular structure of T304 proved that T304 was released and adsorbed to the workpiece surface. After T304 was adsorbed on the surface of the workpiece, it was prone to frictional chemical adsorption on the metal surface, thereby increasing the relative atomic concentration of C and O elements, while the relative concentration of Fe decreased, as shown in Table 4. In addition, there was a clear peak of P on the grinding surface of nano-capsule wheels, while other grinding wheels did not appear, which fully proved the release of T304 during the grinding process [51,52]. P was much higher in MQL grinding with the nano-capsule nanofluid, indicating that the nanofluid effectively penetrated the grinding area and acted as a lubricant.

Figure 17 shows the model of the contact area of the nano-capsule wheel during grinding. The nano-capsules in the grinding wheel released T304 during grinding, which acted together with CNT fragments on the surface of the workpiece to form a more sufficient self-lubricating layer. It has three functions. The first is reducing friction, which provides lubrication between the abrasive particles and the workpiece and reduces the friction coefficient of the resin grinding tool. The second is anti-wear, reducing the adhesion between abrasive particles and chips, reducing the adhesion, blockage, and wear of the grinding tool, maintaining a sharp cutting effect, and improving the grinding ratio. The third is a polishing effect, that is, preventing the grinding debris from entering and causing scratches on the workpiece and improving the surface quality of the workpiece.

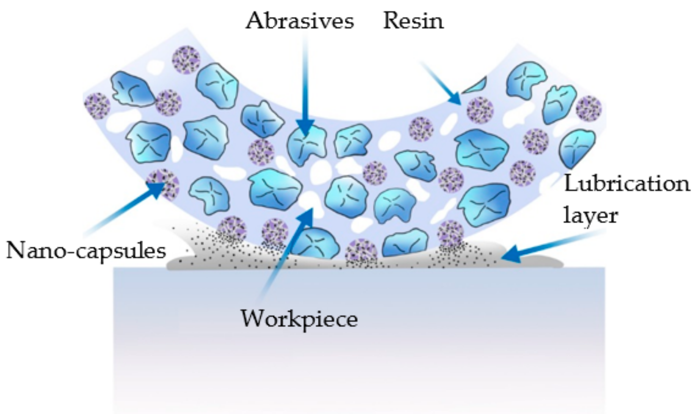

Figure 17. Self-lubrication model of wheels filled with nano-capsules.

Compared with current grinding wheels directly filled with solid lubricants, such as the self-lubricating grinding wheel developed by Shaji et al. [14], the biggest advantage of the grinding wheel prepared in this paper is that it can significantly improve the mechanical strength of the grinding wheel, thereby increasing the grinding speed. This is because filling with solid lubrication can reduce the bonding strength of the bond, while the CNTs@T304 nano-capsules developed in this article can increase the strength of the bond. Compared with the capsule grinding wheels currently developed by Yamaguchi et al. [15], the advantage of the grinding wheel prepared in this article is that it can achieve a uniform release of lubricant, avoid the loss of liquid lubricant caused by the wheel rotation, and thus achieve better cooling and lubrication. Compared with the newly developed grinding wheel filled with cyclodextrin composites of Xu et al. [16], the nano-capsule grinding wheel developed in this research can increase the strength of the wheel by 40%. The grinding force and grinding temperature were reduced by 25% and 32%, respectively, and the grinding ratio of the grinding wheel was increased by 26%.

Compared with the nanofluids prepared by other scholars using common nanoparticles [6–11], the nano-capsules prepared in this paper are characterized by self-lubrication and can significantly improve the dispersion stability, thermal conductivity, and tribological properties of nanofluids. The nano-capsule nanofluid developed in this paper can improve the thermal conductivity by 22% and tribological performance by 15% compared with common nanofluids. The price of the CNT nano-capsules developed in this paper is about 800$/500 g, which may be much more expensive than ordinary graphite or MoS_2 nanoparticles. Therefore, cost is the main factor limiting the application of nano-capsules. In addition, the current filling rate of nano-capsules is small, which limits the self-lubricating performance of grinding wheels and nanofluids. Therefore, subsequent research needs to continuously improve the filling rate, so that a better grinding performance of grinding wheels and nanofluids will be achieved.

5. Conclusions

(1) CNTs@T304 nano-capsules are successfully prepared with a filling rate of about 25% and demonstrated to be thermally stable with TG and DSC analysis. Nanofluids prepared with nano-capsules exhibit better thermal conductivity, dispersion stability, and wetting properties.

(2) CNTs@T304 nano-capsules can adequately resist the curing temperature of the wheel, and their structure is not damaged during the curing process. The mechanical properties can meet the actual conditions when the filling amount is within a certain range.

(3) Compared with a common wheel, the grinding force and grinding temperature were reduced by 24% and 28%, respectively, and the surface roughness of the workpiece and the grinding ratio were increased by 18% and by 21%, respectively, when grinding GCr15 steel with the nano-capsule wheel.

(4) As the grinding speed increases, the grinding force and temperature of nano-capsule grinding wheels also tend to decrease, but the grinding ratio does not change much. Lubrication with nanofluids could further reduce the grinding force, grinding temperature, and surface roughness values.

(5) During the grinding process, T304 is released from the wheel filled with nano-capsules, which adsorbs onto the surface of the workpiece and works together with CNTs to form a lubricating layer. The surface layer in the contact area formed under the synergistic effect acts to reduce friction, resist wear, and improve the surface quality.

Author Contributions: Conceptualization, J.G. and S.H.; methodology, Z.Z.; software, L.Y.; validation, J.G., Y.X. and X.X.; formal analysis, L.Y.; investigation, L.Y.; resources, S.H.; data curation, L.Y.; writing—original draft preparation, Z.Z.; writing—review and editing, J.G.; visualization, L.Y.; supervision, J.G.; project administration, L.Y.; funding acquisition, J.G. and S.H. All authors have read and agreed to the published version of the manuscript.

Funding: This research was financially supported by the Youth Science Foundation Program of the Natural Science Foundation of China (NSFC 51805345), the Natural Science Foundation of Hebei Province (Grant No. E2022203123), and the Hebei Provincial Research Foundation for Returned Scholars (Grant No. C20220335).

Data Availability Statement: The authors confirm that the data supporting the findings of this study are available within the article.

Conflicts of Interest: The authors declare no conflict of interest.

References

1. Abrão, B.S.; Pereira, M.F.; da Silva, L.R.R.; Machado, Á.R.; Gelamo, R.V.; de Freitas, F.M.C.; Mia, M.; da Silva, R.B. Improvements of the MQL Cooling-Lubrication Condition by the Addition of Multilayer Graphene Platelets in Peripheral Grinding of SAE 52,100 Steel. *Lubricants* **2021**, *9*, 79. [CrossRef]
2. Saravanapriyan, S.N.A.; Vijayaraghavan, V.; Krishnamurthy, R. Significance of grinding burn on high speed steel tool performance. *J. Mater. Process. Technol.* **2003**, *134*, 166–173. [CrossRef]
3. Kota, S.S.; Balguri, P.K.; Govardhan, D. Optimization of grinding depth to avoid grind-induced burns in 35NCD16 alloy. *Mater. Today Proc.* **2022**, *62*, 2739–2743. [CrossRef]
4. Lightstone, M.; Koshy, P.; Tullis, S. High-coherence jets for focused fluid delivery in grinding. *CIRP Ann.* **2021**, *70*, 293–296. [CrossRef]
5. Peng, R.; Zhao, L.; Tang, X.; Xiao, X.; Gao, J. Heat transfer performance assessment of abrasive phyllotaxy arrangement in internal cooling grinding. *Int. J. Heat Mass Transf.* **2022**, *197*, 123317. [CrossRef]
6. Shah, R.; Shirvani, K.A.; Przyborowski, A.; Pai, N.; Mosleh, M. Role of Nanofluid Minimum Quantity Lubrication (NMQL) in Machining Application. *Lubricants* **2022**, *10*, 266–281. [CrossRef]
7. Oliveira, D.d.J.; Guermandi, L.G.; Bianchi, E.C.; Diniz, A.E.; de Aguiar, P.R.; Canarim, R.C. Improving minimum quantity lubrication in CBN grinding using compressed air wheel cleaning. *J. Mater. Process. Technol.* **2012**, *212*, 2559–2568. [CrossRef]
8. Shen, B.; Malshe, A.P.; Kalita, P.; Shih, A.J. Performance of novel MoS_2 nanoparticles based grinding fluids in minimum quantity lubrication grinding. *Trans. NAMRI/SME* **2008**, *36*, 357–364.
9. Zhang, D. Experimental evaluation of the lubrication performance of MoS_2/CNT nanofluid for minimal quantity lubrication in Ni-based alloy grinding. *Int. J. Mach. Tools Manuf. Des. Res. Appl.* **2015**, *99*, 19–33. [CrossRef]
10. Zhang, Y.; Li, C.; Jia, D.; Zhang, D.; Zhang, X. Experimental evaluation of MoS_2 nanoparticles in jet MQL grinding with different types of vegetable oil as base oil. *J. Clean. Prod.* **2015**, *87*, 930–940. [CrossRef]
11. Wang, Y.; Li, C.; Zhang, Y.; Li, B.; Yang, M.; Zhang, X.; Guo, S.; Liu, G. Experimental evaluation of the lubrication properties of the wheel/workpiece interface in MQL grinding with different nanofluids. *Tribol. Int.* **2016**, *99*, 198–210. [CrossRef]
12. Hwang, Y.; Lee, J.K.; Lee, C.H.; Jung, Y.M.; Cheong, S.I.; Lee, C.G.; Ku, B.C.; Jang, S.P. Stability and thermal conductivity characteristics of nanofluids. *Thermochim. Acta* **2007**, *455*, 70–74. [CrossRef]
13. Hwang, Y.; Lee, J.-K.; Lee, J.-K.; Jeong, Y.-M.; Cheong, S.-i.; Ahn, Y.-C.; Kim, S.H. Production and dispersion stability of nanoparticles in nanofluids. *Powder Technol.* **2008**, *186*, 145–153. [CrossRef]
14. Shaji, S.; Radhakrishnan, V. An investigation on solid lubricant moulded grinding wheels. *Int. J. Mach. Tools Manuf.* **2003**, *43*, 965–972. [CrossRef]
15. Toshiyuki, E.; Yutaka, S.; Yasuhiro, T. Mechanical-chemical finishing using a lapping stone including microcapsules. *Trans. Jpn. Soc. Mech. Eng. Ser.* **1999**, *65*, 394–399.
16. Xu, X.; Huang, S.; Guan, J.; Hu, J.; Peng, W. Grinding performance and self–lubrication mechanism of phenolic resin-bonded grinding wheel filled with inclusion complex of β-cyclodextrin and dialkyl pentasulfide. *J. Mater. Process. Technol.* **2015**, *221*, 163–171. [CrossRef]
17. Iijima, J. Helical microtubules of graphitic carbon. *Nature* **1991**, *354*, 56–58. [CrossRef]
18. Thostenson, E.T.; Ren, Z.; Chou, T.W. Advances in the science and technology of carbon nanotubes and their composites: A review. *Compos. Sci. Technol.* **2001**, *61*, 1899–1912. [CrossRef]
19. Wu, M.; Liu, C.; Sun, R.; Yu, T.; Li, Y.; Yang, G. Carbon nanofiber activated by molybdenum disulfide as an effective binder-free composite anode for highly reversible lithium storage. *Int. J. Energy Res.* **2020**, *44*, 4605–4615. [CrossRef]
20. Kong, F.; He, X.; Chen, J.; Tao, S.; Luo, H. Hierarchical $Ni(HCO_3)_2$ Nanosheets Anchored on Carbon Nanofibers as Binder-Free Anodes for Lithium-Ion Batteries. *Energy Technol.* **2019**, *7*, 1900094. [CrossRef]
21. Jang, B.-K.; Sakka, Y. Dispersion and Shortening of Multi-Walled Carbon Nanotubes by Size Modification. *Mater. Trans.* **2010**, *51*, 192–195. [CrossRef]
22. Jehhef, K.A.; Siba, M.A.A.A. Effect of surfactant addition on the nanofluids properties: A review. *Acta Mech. Malays.* **2019**, *2*, 1–19. [CrossRef]
23. Huaxu, L.; Fuqiang, W.; Dong, L.; Jie, Z.; Jianyu, T. Optical properties and transmittances of ZnO-containing nanofluids in spectral splitting photovoltaic/thermal systems. *Int. J. Heat Mass Transf.* **2019**, *128*, 668–678. [CrossRef]
24. Safiei, W.; Rahman, M.M.; Yusoff, A.R.; Radin, M.R. Preparation, stability and wettability of nanofluid: A review. *J. Mech. Eng. Sci.* **2020**, *14*, 7244–7257. [CrossRef]
25. Zhang, Y.; Liu, Z.; Yang, L.; Xiong, Y. Microstructure and shear property of Ni-coated carbon nanotubes reinforced InSn-50Ag composite solder joints prepared by transient liquid phase bonding. *J. Manuf. Process.* **2022**, *73*, 177–182. [CrossRef]
26. Zhou, Z.; Feng, Y.; Xu, W.; Zhou, H.; Qin, Y.; Jia, X. Experimental study on longitudinal-torsional ultrasonic vibration drilling of carbon fiber–reinforced plastics/titanium alloy stacks. *Int. J. Adv. Manuf. Technol.* **2023**, *124*, 527–543. [CrossRef]

27. Wu, J.; Liu, T.; Wang, K.; Sørby, K. A measuring method for micro force based on MEMS planar torsional spring. *Meas. Sci. Technol.* **2020**, *32*, 035002. [CrossRef]
28. Liao, Y.; Zhang, F.; Li, K.; Wu, S. Grinding performance of micro-texured grinding wheel on different ceramic materials. *Diam. Abras. Eng.* **2022**, *42*, 290–299.
29. Sun, Y.; Zhu, T.; Cai, M.; Zhang, Y.; Fan, C.; An, Z. Influence of grinding lubrication methods on surface integrity of nickel-based single crystal superalloy. *Diam. Abras. Eng.* **2022**, *42*, 201–207.
30. Zhou, H.; Feng, Y.; Xu, W.; Zhou, Z.; Qin, Y.; Jia, X. Experimental research on new hole-making method assisted with asynchronous mixed frequency vibration in TiBw/TC_4 composites. *Int. J. Adv. Manuf. Technol.* **2022**, *125*, 543–561. [CrossRef]
31. Li, Z.; He, C.; Song, W.; Wu, Y.; Liu, Y.; Feng, J.; Yang, J.; Song, Y. Optical limiting properties of hybrid nickel naphthalocyanine-titania nanoparticals thin films. *Opt. Laser Technol.* **2019**, *112*, 413–419. [CrossRef]
32. Li, M.; Zhao, Y.; Fang, J.; Zhao, S.; Xu, G.; Wang, Z. Effect of dimethyl carbonate on the micromorphology and structure of combustion particles from diesel engines. *Energy Sources Part Recovery Util. Environ. Eff.* **2019**, *42*, 1155–1165. [CrossRef]
33. Dujardin, E.; Ebbesen, T.W.; Hiura, H.; Tanigaki, K. Capillarity and Wetting of Carbon Nanotubes. *Science* **1994**, *265*, 1850–1852. [CrossRef]
34. Babita, S.S.; Gupta, S.M. Synergic effect of SDBS and GA to prepare stable dispersion of CNT in water for industrial heat transfer applications. *Mater. Res. Express* **2018**, *5*, 055511. [CrossRef]
35. Zhao, Y.; Xu, G.; Li, M.; Chen, Q. Effects of exhaust gas recirculation composition and temperature on microscopic mechanical properties of particles in a diesel engine. *Environ. Prog. Sustain. Energy* **2018**, *38*, e13037. [CrossRef]
36. Xuan, Y.; Li, Q. Heat transfer enhancement of nanofluids. *Int. J. Heat Fluid Flow* **2000**, *21*, 58–64. [CrossRef]
37. Song, Y.; Yu, Z.; Liu, Y.; Dong, L.; Ma, H. A Hierarchical Conical Array with Controlled Adhesion and Drop Bounce Ability for Reducing Residual Non-Newtonian Liquids. *J. Bionic Eng.* **2021**, *18*, 12–21. [CrossRef]
38. Tanvir, S.; Li, Q. Surface Tension of Nanofluid-type Fuels containing Suspended Nanomaterials. *Nanoscale Res. Lett.* **2012**, *7*, 226–236. [CrossRef]
39. Zhang, D.; Kuang, Y.; Hong, X.; Liu, Y.; Yang, X. Plasmon enhancement of optical absorption in ultra-thin film solar cells by rear located aluminum nanodisk arrays. *Opt. Quantum Electron.* **2017**, *49*, 161–169. [CrossRef]
40. Khaleduzzaman, S.S.; Mahbubul, I.M.; Shahrul, I.M.; Saidur, R. Effect of particle concentration, temperature and surfactant on surface tension of nanofluids. *Int. Commun. Heat Mass Transf. Rapid Commun. J.* **2013**, *49*, 110–114. [CrossRef]
41. Zhang, D.; Yang, X.; Hong, X.; Liu, Y.; Feng, J. Scattering of light into thin film solar cells by rear located hemispherical silver nanoparticles. *Opt. Quantum Electron.* **2016**, *48*, 120–126. [CrossRef]
42. Yang, C. Research on abrasive wear dress of CBN honing tool based on single abrasive cutting. *Diam. Abras. Eng.* **2022**, *42*, 728–737.
43. Xu, G.; Zhao, Y.; Li, M.; Lin, L.; Hu, Y. Effects of the lubricating oil and diesel mixture combustion on the oxidation and microphysical properties of particulate matter. *Energy Rep.* **2020**, *6*, 308–314. [CrossRef]
44. Wu, J.; Liu, T.; Yu, N.; Cao, J.; Wang, K.; Sørby, K. A Pin-on-Disk Tribometer for Friction and Lubricating Performance in mm-Scale. *Tribol. Lett.* **2021**, *69*, 36–42. [CrossRef]
45. Zhao, Y.; Xu, G.; Li, M.; Chen, Q. The evolution of the micro-morphology and micro-structure of particles from diesel engine in combination with exhaust gas recirculation. *Energy Sources Part Recovery Util. Environ. Eff.* **2018**, *40*, 805–820. [CrossRef]
46. Zhang, W.; Shen, Y.; Yan, Y.; Guo, R.; Guan, W.; Guo, G. Microstructure characterization and mechanical behavior of dissimilar friction stir welded Al/Cu couple with different joint configurations. *Int. J. Adv. Manuf. Technol.* **2017**, *94*, 1021–1030. [CrossRef]
47. Jiang, B.; Yuan, H.; Dang, Q.; Wang, T.; Pang, T.; Cheng, Y.; Wu, K.; Wu, X.; Shao, M. Quantitative evaluation of synergistic effects for Pt nanoparticles embedded in N-enriched carbon matrix as an efficient and durable catalyst for the hydrogen evolution reaction and their PEMWE performance. *Int. J. Hydrogen Energy* **2019**, *44*, 31121–31128. [CrossRef]
48. Shen, Z.; Geng, F.; Fan, X.; Shen, Z.; Wang, H. Effect of preparation process on elevated temperature tribological properties of composite polyurea grease. *Ind. Lubr. Tribol.* **2016**, *68*, 611–616. [CrossRef]
49. Xu, G.; Zhao, Y.; Li, M.; Lin, L.; Hu, Y. Effects of Lubricating Oil Additives on the Microphysical Properties of Diesel Exhaust Particulate Matter. *Combust. Sci. Technol.* **2020**, *193*, 1718–1733. [CrossRef]
50. Zhao, W.; Li, J.; She, T.; Ma, S.; Cheng, Z.; Wang, G.; Zhao, P.; Wei, W.; Xia, D.; Leung, D.Y.C. Study on the Photocatalysis Mechanism of the Z-Scheme Cobalt Oxide Nanocubes/Carbon Nitride Nanosheets Heterojunction Photocatalyst with High Photocatalytic Performances. *J. Hazard Mater.* **2021**, *402*, 123839. [CrossRef]
51. Wang, T.; Li, X.; Pang, Y.; Gao, X.; Kou, Z.; Tang, J.; Wang, J. Unlocking the synergy of interface and oxygen vacancy by core-shell nickel phosphide@oxyhydroxide nanosheets arrays for accelerating alkaline oxygen evolution kinetics. *Chem. Eng. J.* **2021**, *425*, 131491. [CrossRef]
52. Oumahi, C.; Mogne, T.L.; Aguilar-Tapia, A.; Charrin, C.; Geantet, C.; Afanasiev, P.; Thiebaut, B.; De Barros-Bouchet, M.I. Impact of Fatty Triamine on Friction Reduction Performance of MoDTC Lubrication Additive. *Lubricants* **2022**, *10*, 365–371. [CrossRef]